

Thermal and structural properties of ionic fluids

Hendrik Bartsch,^{*} Oliver Dannenmann, and Markus Bier[†]

*Max-Planck-Institut für Intelligente Systeme, Heisenbergstr. 3,
70569 Stuttgart, Germany, and Institut für Theoretische Physik IV,
Universität Stuttgart, Pfaffenwaldring 57, 70569 Stuttgart, Germany*

(Dated: 15 April 2015)

The electrostatic interaction in ionic fluids is well-known to give rise to a characteristic phase behavior and structure. Sometimes its long range is proposed to single out the electrostatic potential over other interactions with shorter ranges. Here the importance of the range for the phase behavior and the structure of ionic fluids is investigated by means of grandcanonical Monte Carlo simulations of the lattice restricted primitive model (LRPM). The long-ranged electrostatic interaction is compared to various types of short-ranged potentials obtained by sharp and/or smooth cut-off schemes. Sharply cut off electrostatic potentials are found to lead to a strong dependence of the phase behavior and the structure on the cut-off radius. However, when combined with a suitable additional smooth cut-off, the short-ranged LRPM is found to exhibit quantitatively the same phase behavior and structure as the conventional long-ranged LRPM. Moreover, the Stillinger-Lovett perfect screening property, which is well-known to be generated by the long-ranged electrostatic potential, is also fulfilled by short-ranged LRPMs with smooth cut-offs. By showing that the characteristic phase behavior and structure of ionic fluids can also be found in systems with short-ranged potentials, one can conclude that the decisive property of the electrostatic potential in ionic fluids is not the long range but rather the valency dependence.

I. INTRODUCTION

Over the last two decades, the scientific interest in organic salts with melting points near room temperature, so-called room temperature ionic liquids (RTILs), has been growing steadily. Features such as a negligible vapor pressure and a remarkable thermal stability [1–4] promise future applications as solvents for syntheses, electrolytes in fuel cells, solar cells, and batteries, as well as in biomass processing [5–10]. Moreover, due to the tiny vapor pressure many applications are conceivable under ultrahigh vacuum [1, 3, 11, 12]. However, the technological use of RTILs requires an in-depth understanding of ionic systems.

The Coulomb interaction, underlying these systems, acts repulsively for equally-charged and attractively for oppositely-charged ions and it decays $\propto 1/r$, i.e., it is long-ranged. On the other hand, the pair distribution functions of an ionic fluid decay exponentially, which is called the Stillinger-Lovett perfect screening property [13–16] and which is a necessary consequence of the long range of the Coulomb potential [17, 18]. It is a challenge for more than a century now to develop quantitatively reliable theoretical descriptions of this peculiar combination of properties. For dilute electrolyte solutions Debye-Hückel theory [19–21] is typically a good starting point, whereas for dense ionic systems ion-pairing is relevant [13, 14]. From experimental work [22–25] as well as continuum simulations [26–29], there is evidence that in particular the critical behavior of ionic systems is very similar to the Ising universality class, which typically ap-

plies to systems with short-ranged interactions. This result suggests that the long-range character of the bare Coulomb potential might be of minor importance for the critical properties of ionic fluids.

The aim of the present work is to investigate the relevance of the long range of the Coulomb interaction for the whole phase diagram and the bulk structure. This is done by studying the lattice restricted primitive model (LRPM) for the Coulomb potential being truncated smoothly on a length scale $1/\alpha$ and sharply at a cut-off radius r_{cut} . The technical details of the model and the approach are presented in Sec. II. The long-ranged LRPM is well-known to exhibit tricritical behavior at the crossover from a first- to a second-order phase transition between a charge-ordered and a charge-disordered phase [30, 31]. The (L)RPM renders the ions as homogeneous charged hard spheres, which is of course not valid for ionic liquids in general, since they may exhibit charge as well as shape anisotropy. However, this work is concerned with the influence of the long range and the valency dependence of the electrostatic interaction, being omnipresent in all kinds of ionic systems. In particular, the impact of the long range will not depend on rather short-range features like charge or shape anisotropy, therefore we consider this simple model of ionic fluids as sufficient for the present investigation. It is shown in Sec. III that, upon varying the smooth cut-off decay constant α and the sharp cut-off radius r_{cut} , the short-ranged LRPM can be tuned from a system void of a charged-ordered phase via one exhibiting charge-ordered and charge-disordered phases but differing quantitatively from the long-ranged LRPM to a model with short-ranged interactions whose phase behavior and structure is quantitatively the same as for the long-ranged Coulomb interaction. Moreover, even the Stillinger-Lovett perfect screening property can

^{*} hbartsch@is.mpg.de

[†] bier@is.mpg.de

be fulfilled for suitable smooth cut-off potentials, an observation which is not trivial in the context of short-ranged interactions. By showing that the characteristic phase behavior and structure of ionic fluids can also be found in systems with short-ranged potentials, it is concluded in Sec. IV that the decisive property of the electrostatic potential in ionic fluids is not the long range but rather the valency dependence.

II. MODEL AND METHOD

A. LRPM with truncated Coulomb potential

Consider the lattice restricted primitive model (LRPM) of univalent cations (valency $z_{\oplus} = +1$) and anions (valency $z_{\ominus} = -1$) with hard cores of diameter σ occupying but not necessarily exhausting the sites of a three-dimensional simple cubic lattice with lattice constant σ . Global charge neutrality is guaranteed by an equal number of cations and anions in the system, and the hard cores ensure that each site is either empty or singly occupied. Within the original LRPM two ions of species $i, j \in \{\oplus, \ominus\}$ at a distance r interact, besides the hard core exclusion, via the infinitely-ranged Coulomb potential $\frac{l_b z_i z_j}{r}$, where $l_b = \frac{e^2}{4\pi\epsilon kT}$ is the Bjerrum length with the electronic permittivity ϵ , the Boltzmann constant k , and the temperature T , and where r is measured with the Euclidean metric.

In the present work the relevance of the long-range character of the Coulomb interaction for the properties of ionic systems is studied by considering the implications of replacing the infinitely-ranged Coulomb potential by the truncated Coulomb-like potential

$$\beta\phi_{p,q}(\mathbf{r}, z_i, z_j) = \begin{cases} \frac{l_b z_i z_j}{\|\mathbf{r}\|_p} \operatorname{erfc}(\alpha\|\mathbf{r}\|_p) & , \|\mathbf{r}\|_q \leq r_{\text{cut}} \\ 0 & , \|\mathbf{r}\|_q > r_{\text{cut}} \end{cases} \quad (1)$$

with the inverse temperature $\beta = 1/(kT)$, the decay constant $\alpha \geq 0$, and the cut-off radius r_{cut} . By means of Eq. (1) two different methods of cutting off the Coulomb potential can be studied: On the one hand, the factor $\operatorname{erfc}(\alpha\|\mathbf{r}\|_p)$, leads to a smooth cutting off on the length scale $1/\alpha$, and, on the other hand, a sharp cutting off at radius $\|\mathbf{r}\|_q = r_{\text{cut}}$ can be considered. Inspired by the short-ranged potentials appearing within the Ewald method [32], here the smoothening factors are chosen to be complementary error functions $\operatorname{erfc}(x) = 2/\pi \int_x^\infty d\tau \exp(-\tau^2)$. Obviously, the infinitely-ranged Coulomb potential corresponds to $\alpha = 0, r_{\text{cut}} = \infty$. Besides the Euclidean norm $\|\mathbf{r}\|_2 = \sqrt{x^2 + y^2 + z^2}$ to measure distances, the 1-norm $\|\mathbf{r}\|_1 = |x| + |y| + |z|$ and the supremum norm $\|\mathbf{r}\|_\infty = \max(|x|, |y|, |z|)$ are considered, which are more adapted to a lattice model since, for lattice vectors \mathbf{r} , they lead to values which are integer multiples of the lattice constant σ . Since all norms

are equivalent in finite dimensions, the power law $\propto 1/r$ is asymptotically preserved irrespective of the choice of the norm. The parameters p and q in Eq. (1) describe the norms to be used for measuring the distance determining the interaction potential and the sharp cut-off, respectively.

B. Grandcanonical Monte Carlo simulations

In order to discuss the thermal and structural properties of the LRPM with the truncated Coulomb-like interaction Eq. (1), the packing fraction η and the pair distribution functions $g_{ij}(r)$, $i, j \in \{\oplus, \ominus\}$, are determined for cubic boxes $\mathcal{V} := \{0, \sigma, \dots, (L-1)\sigma\}^3$, $L \in \mathbb{N}$, with periodic boundary conditions using grandcanonical Monte Carlo simulations. The set of all configurations ζ of cations and anions occupying \mathcal{V} can be expressed as the set of all maps $\zeta : \mathcal{V} \rightarrow \{0, z_{\oplus}, z_{\ominus}\}$, which result in the charge $\zeta(\mathbf{r}) \in \{0, z_{\oplus}, z_{\ominus}\}$ located at position $\mathbf{r} \in \mathcal{V}$, i.e., $\zeta(\mathbf{r}) = 0$ iff site \mathbf{r} is empty, $\zeta(\mathbf{r}) = z_{\oplus}$ iff site \mathbf{r} is occupied by a cation, and $\zeta(\mathbf{r}) = z_{\ominus}$ iff site \mathbf{r} is occupied by an anion. Standard Metropolis importance sampling of the grandcanonical Boltzmann distribution $P(\zeta) \propto \exp(\beta\mu N[\zeta] - \beta H[\zeta])$ with the chemical potential μ , the total number of ions $N[\zeta] = N_{\oplus}[\zeta] + N_{\ominus}[\zeta]$, and the Hamiltonian

$$\beta H[\zeta] = \frac{1}{2} \sum_{\substack{\mathbf{r}, \mathbf{r}' \in \mathcal{V} \\ \mathbf{r} \neq \mathbf{r}'}} \beta \phi_{p,q}(\mathbf{r} - \mathbf{r}', \zeta(\mathbf{r}), \zeta(\mathbf{r}')) \quad (2)$$

on the set of all charge-neutral configurations ζ is applied. Charge neutrality is preserved during the simulation runs due to insertions and removals of only neutral pairs of cations and anions, i.e., the number of cations $N_{\oplus}[\zeta]$ equals the number of anions $N_{\ominus}[\zeta]$.

The packing fraction is the average

$$\eta = \frac{\langle N[\zeta] \rangle}{L^3} \quad (3)$$

and the pair distribution functions are given by

$$g_{i,j}(r) = \frac{4\langle N_{i,j}(r, [\zeta]) \rangle}{V_{\text{shell}}(r) L^3 \eta^2} \quad (4)$$

with $i, j \in \{\oplus, \ominus\}$, r being a distance measured in the 1-norm, $V_{\text{shell}}(r) = 4(r/\sigma)^2 + 2$ representing the number of all sites in the shell of 1-norm distance r around a site, and $N_{i,j}(r, [\zeta])$ denoting the total number of all ordered pairs $(\mathbf{r}_i, \mathbf{r}_j)$ of positions $\mathbf{r}_i, \mathbf{r}_j \in \mathcal{V}$ being separated by a 1-norm distance $r = \|\mathbf{r}_i - \mathbf{r}_j\|_1$ and such that an ion of species i is located at position \mathbf{r}_i and an ion of species j is located at position \mathbf{r}_j . Here the pair distribution functions $g_{i,j}(r)$ are defined in terms of 1-norm distances r because, for the present simple-cubic lattice geometry, this choice is most convenient in order to distinguish charge-ordered and charge-disordered phases.

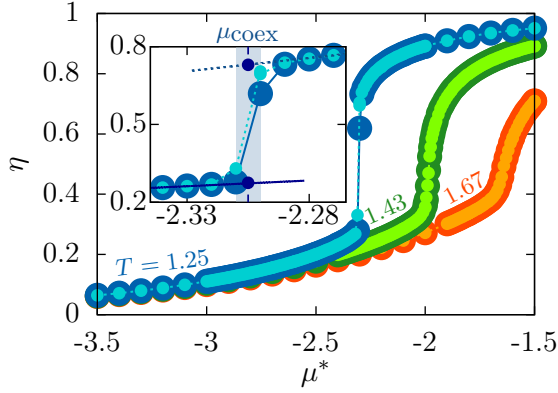


FIG. 1. Isotherms $T^* \in \{1.25, 1.43, 1.67\}$ for $L = 12, \alpha = 0, r_{\text{cut}}/\sigma = 1$ using the 1-norm ($p = q = 1$) in Eq. (2). For $T^* = 1.25$ a distinct discontinuity of the packing fraction η at chemical potential $\mu^* \approx -2.3$ can be observed, while for $T^* = 1.67$ a continuous curve occurs. Therefore, the critical temperature T_c^* , where the first-order gas/liquid phase transition associated with the discontinuity of the packing fraction η terminates, is located within this temperature range: $T_c^* \in [1.25, 1.67]$. For each isotherm two sets of data points are shown, which correspond to either an initially empty system (large dots connected by solid lines) or an initially totally filled system (small dots connected by dashed lines). The inset sketches the procedure to estimate the packing fractions at coexistence (see Sec. II C).

The equilibrium state of the LRPM is determined by the choice of the (dimensionless) temperature $T^* := \sigma/l_b$ and the (dimensionless) chemical potential $\mu^* := \beta\mu$. Within the present work we considered temperatures and chemical potentials in the ranges $T^* \in [0.04, 10]$ and $\mu^* \in [-8, 0]$, respectively. Box sizes were varied in the range $L \in \{8, \dots, 19\}$.

From an analysis of the equation of state, which are investigated as isotherms in η - μ^* -space, and of the structure in terms of the pair distribution functions the phase diagram of the LRPM for various sets of values of the decay constant α and of the cut-off radius r_{cut} are inferred. The following subsections explain the procedures to estimate the locations of the binodals of the first-order gas/liquid phase transition and of the so-called λ -line of the continuous phase transition between the charge-ordered and the charge-disordered phase.

C. Estimation of the binodals

Estimates of the binodals of the first-order gas/liquid phase transition are obtained by determining the equation of state $\eta(T^*, \mu^*)$. Figure 1 displays isotherms $T^* \in \{1.25, 1.43, 1.67\}$ for $L = 12, \alpha = 0, r_{\text{cut}}/\sigma = 1$ using the 1-norm ($p = q = 1$) in Eq. (2). For the lowest temperature $T^* = 1.25$ a discontinuity in the packing fraction $\eta(\mu^*)$ indicates a first-order gas/liquid phase transition, whereas for the highest temperature $T^* = 1.67$ no

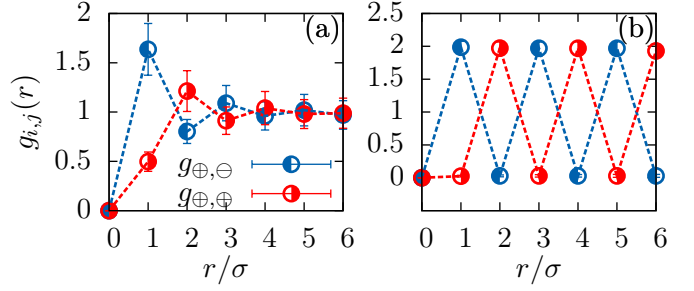


FIG. 2. Pair distribution functions for $L = 12, \alpha = 0, r_{\text{cut}}/\sigma = 1$ using the 1-norm ($p = q = 1$) in Eq. (2) at temperature $T^* = 2$ and packing fraction $\eta = 0.37$ (a) and $\eta = 0.90$ (b). The red curves represent the pair distribution function for equally charged ions, while the blue curves represent those of oppositely charged ions. Panel (a) shows the structure of the charge-disordered phase, which is characterized by a rapid vanishing of the spatial correlations. Panel (b) displays the case of the charge-ordered phase, where correlations are long-ranged due to a shell-wise alternating distribution of cations and anions.

gas/liquid phase transition occurs. An estimate of the critical temperature T_c^* is obtained as a temperature for which $\eta(\mu^*)$ is discontinuous for $T^* < T_c^*$ and continuous for $T^* > T_c^*$. This simple method is sufficiently precise for the present purpose.

In order to estimate the binodal packing fractions $\eta_1(T^*)$ and $\eta_2(T^*)$ of gas/liquid coexistence at a temperature $T^* < T_c^*$ the phase transition is first located within a range of the chemical potentials μ^* which is as narrow as possible and outside which the well-known hysteresis effect of first-order phase transitions does not occur. For $T^* = 1.25$ in Fig. 1, e.g., the inset leads to the range $\mu^* \in [-2.33, -2.28]$. Our estimate of the chemical potential $\mu_{\text{coex}}^*(T^*)$ at coexistence is the mid-point of the μ^* -interval of steepest increase of the packing fraction $\eta(\mu^*)$. For the isotherm depicted in the inset of Fig. 1, this choice yields $\mu_{\text{coex}}^*(T^*) \approx -2.305$ for $T^* = 1.25$. Estimates of the binodal packing fractions $\eta_1(T^*)$ and $\eta_2(T^*)$ are obtained by linearly extrapolating the hysteresis-free parts of $\eta(\mu^*)$ to $\mu^* = \mu_{\text{coex}}^*(T^*)$ from below and from above, respectively. For Fig. 1, e.g., these estimates are $\eta_1(T^*) \approx 0.27$ and $\eta_2(T^*) \approx 0.73$ for $T^* = 1.25$. Again, this simple method is sufficiently precise, since, for the purpose of the present work, the location of the binodals is required to be known only semi-quantitatively but not to the highest technically feasible accuracy. More sophisticated and thus precise methods, such as umbrella sampling techniques or methods based on finite-size scaling and histogram reweighting [33, 34], are not required here.

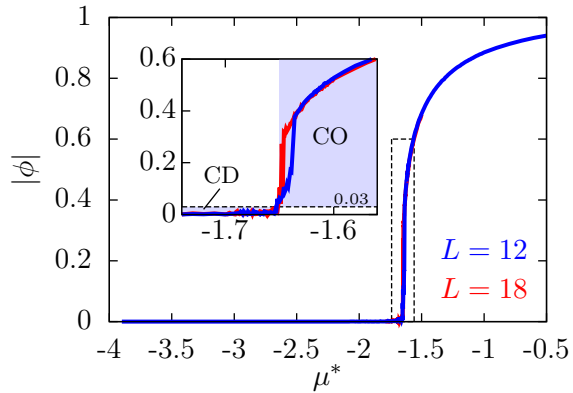


FIG. 3. Order parameter $|\phi|$ as a function of the chemical potential μ^* for decay constant $\alpha = 0$, cut-off radius $r_{\text{cut}}/\sigma = 1$ using the 1-norm ($p = q = 1$) in Eq. (2), and temperature $T^* = 1.67$ for box sizes $L \in \{12, 18\}$. It signals the second-order phase transition between the charge-disordered (CD) phase, where $|\phi| \approx 0$, and the charge-ordered (CO) phase, where $|\phi| \approx 0$. In order to account for finite-size effects, the convention is adopted that the phase transition occurs at $|\phi| = 0.03$, which is located at $\mu^* \approx -1.65$ here.

D. Estimation of the λ -line

The structure of the charge-ordered and charge-disordered phase can be observed by analyzing the pair distribution functions $g_{i,j}(r)$ (see Eq. (4)). Figure 2 shows the respective structures of both phases for the case $T^* = 2, L = 12, \alpha = 0, r_{\text{cut}}/\sigma = 1$ using the 1-norm ($p = q = 1$) in Eq. (2). For the charge-disordered phase, spatial correlations vanish rapidly, while for the charge-ordered phase one observes long-ranged correlations due to a shell-wise alternating assembly of cations and anions.

In order to locate the charge-ordered/charge-disordered phase transition, i.e., the λ -line, in the phase diagram, the so-called staggered order parameter

$$\phi := \left\langle \frac{1}{L^3} \sum_{\mathbf{r} \in \mathcal{V}} (-1)^{\|\mathbf{r}\|_1} \zeta(\mathbf{r}) \right\rangle \quad (5)$$

is considered. $|\phi|$ is positive in the charge-ordered phase and it vanishes in the charge-disordered phase. In order to account for finite-size effects, the convention is adopted that a thermodynamic state belongs to the charge-disordered phase iff $|\phi| < 0.03$. Obviously, this convention is largely arbitrary, but it allows a sufficiently precise localization of the λ -line. Figure 3 displays $|\phi|$ as a function of the chemical potential μ^* for decay constant $\alpha = 0$, cut-off radius $r_{\text{cut}}/\sigma = 1$ and temperature $T^* = 1.67$ for box sizes $L \in \{12, 18\}$. For this example, the second-order phase transition, which is expected to belong to the Ising universality class [35], is located at $\mu^* \approx -1.65$.

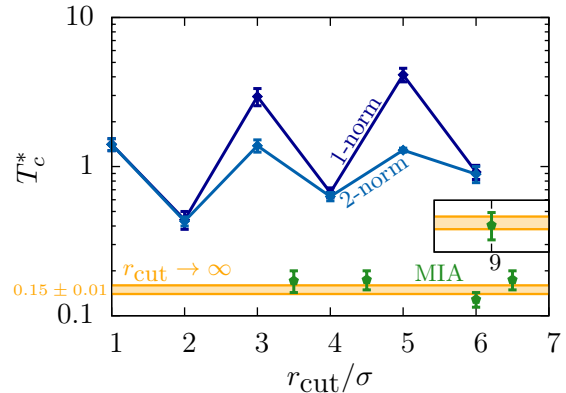


FIG. 4. Critical temperature T_c^* as a function of the cut-off radius r_{cut} for sharp cut-off truncation schemes, where the decay constant $\alpha = 0$ is used in Eq. (1). Data points labeled by '1-norm' and '2-norm' are obtained by truncation of the Coulomb potential at distances $r_{\text{cut}}/\sigma \leq (L - 1)/2$, where all distances are measured in the respective norms, i.e., $p = q$ (see Sec. III A). Moreover, the values within the minimum image approximation ('MIA') are displayed, which corresponds to $p = 2, q = \infty, r_{\text{cut}}/\sigma = (L - 1)/2$ (see Sec. III B). By comparison with the critical temperature $\Theta_c^* \in [0.14, 0.16]$ for the long-ranged Coulomb potential ($r_{\text{cut}} = \infty$) one observes that the MIA results match the long-range value very well, whereas the 1-norm and the 2-norm results largely overestimate the critical temperature.

III. RESULTS AND DISCUSSION

A. Sharp cut-off schemes

In this subsection a sharp cutting off of the Coulomb potential, i.e., $\alpha = 0$ in Eq. (1), is considered with cut-off radii $r_{\text{cut}}/\sigma \leq (L - 1)/2$. First, the discussion is concerned with the dependence of the critical temperature T_c^* on the cut-off radius r_{cut} , which is obtained following the procedure described in Subsec. II C.

Figure 4 compares T_c^* using the 1-norm ($p = q = 1$) and the 2-norm ($p = q = 2$) in Eq. (2) with the critical temperature $\Theta_c^* \in [0.14, 0.16]$ of the long-ranged Coulomb system, i.e., for $r_{\text{cut}} = \infty$ [30, 31, 36]. Distinct oscillations of T_c^* for both 1-norm and 2-norm can be observed, where the amplitude of the latter is much smaller than that of the former. For both metrics, no signs of convergence of T_c^* towards the value Θ_c^* of the long-ranged potential are observable within the considered range of cut-off radii r_{cut} . Moreover, the amplitude of the oscillations appears to even increase for the 1-norm. This odd-even-dependence likewise occurs within the structure for sufficiently large packing fractions: While for odd values of r_{cut}/σ a charge-ordered phase is realized at large packing fractions, no charge-ordering is observed for even values of r_{cut}/σ .

In order to understand the presence or absence of a charge-ordered phase in the case of odd or even values

of r_{cut}/σ , respectively, consider the particular case of the 1-norm metric ($p = q = 1$ in Eq. (2)) and a perfectly charge-ordered configuration ζ_{CO} . The energy of such a configuration is given by (see Eq. (2))

$$\begin{aligned}\beta H[\zeta_{\text{CO}}] &= \frac{L^3}{2T^*} \sum_{i=1}^{r_{\text{cut}}/\sigma} \frac{(-1)^i}{i} V_{\text{shell}}(i\sigma) \\ &= \frac{L^3}{2T^*} \left(-6 + \frac{18}{2} - \frac{38}{3} + \frac{66}{4} - \frac{102}{5} + \dots \right),\end{aligned}\quad (6)$$

where $V_{\text{shell}}(i\sigma) = 4i^2 + 2$ is the number of sites in the i -th shell of 1-norm distance $i\sigma$ around a site. For $r_{\text{cut}}/\sigma = 1$ only nearest neighbors interact and due to $\beta H[\zeta_{\text{CO}}] < 0$ it is energetically favorable for the ions to arrange alternatingly for sufficiently large η . However, for $r_{\text{cut}}/\sigma = 2$ the coions in the second shell overcompensate the contribution of the counterions in the first shell, such that $\beta H[\zeta_{\text{CO}}] > 0$, which renders the charge-ordered phase unfavorable as compared to the charge-disordered phase. This pattern repeats upon increasing r_{cut} with $\beta H[\zeta_{\text{CO}}] < 0$ for odd and $\beta H[\zeta_{\text{CO}}] > 0$ for even values of r_{cut}/σ . Since the size of the i -th shell grows $\propto i^2$ and the strength of the interaction with the central ion decreases $\propto 1/i$, the total energy $\beta H[\zeta_{\text{CO}}]$ oscillates with an amplitude which increases $\propto i$. This growing stability of the charge-ordered phase for odd values of r_{cut}/σ causes the increase in the critical temperature T_c^* for odd-valued cut-off radii. Furthermore, for all cases studied here, it is found that the total energies within the charge-ordered phases for odd-valued cut-off distances are much lower than for the long-ranged Coulomb potential and therefore that the stability of the latter's charge-ordered phase is much weaker. This leads to a significantly lower critical temperature compared to those, obtained using the sharp cut-off scheme. The absence of a charge-ordered phase in the case of even-valued cut-off radii and the increasing deviation of the critical temperature T_c^* from that of the conventional LRPM with long-ranged Coulomb potential, $\Theta_c^* \in [0.14, 0.16]$ in the case of odd-valued cut-off radii leads to the conclusion of some major defect of the sharp cut-off scheme.

Calculations using the 2-norm lead to qualitatively similar results. The quantitative differences for $r_{\text{cut}}/\sigma > 1$ to the case of a 1-norm metric can be attributed to the occurrence of non-integer-valued distances and to the fact that the shells of constant distance from a central site are spheres and not octahedrons. Note, that for the case $r_{\text{cut}}/\sigma = 1$ the distinction between 1-norm and 2-norm is irrelevant. Remarkably, the critical temperatures T_c^* for odd values of r_{cut}/σ are considerably smaller than those for the 1-norm metric, whereas for even values of r_{cut}/σ the differences are very small.

Figure 5 displays the phase diagrams for cut-off radii $r_{\text{cut}}/\sigma \in \{1, 3, 5\}$ (1-norm, $p = q = 1$), which have been determined using the methods presented in Secs. II C and II D. Close to the critical point, the binodals follow a

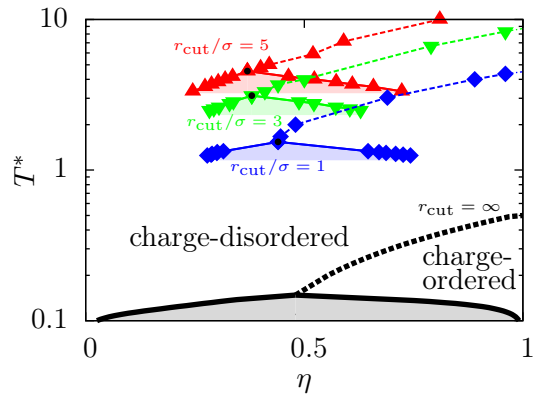


FIG. 5. Phase diagrams for 1-norm metric ($p = q = 1$ in Eq. (2)), decay constant $\alpha = 0$, box size $L = 12$, and cut-off radii $r_{\text{cut}}/\sigma \in \{1, 3, 5\}$ compared with that of the conventional long-ranged LRPM ($r_{\text{cut}} = \infty$ [31]). All these phase diagrams exhibit the same topology of a charge-ordered and a charge-disordered phase separated by a first-order phase transition below and a continuous phase transition above a tricritical point (\bullet). However, for the cases with finite values of the cut-off radius r_{cut} , the tricritical temperature is about an order of magnitude too high and it increases upon increasing r_{cut} .

straight line, which corresponds to the critical exponent $\beta = 1$. Due to this observation and since the λ -line terminates at the critical point, this critical point actually is a *tricritical* point (tagged by a black dot). The long-ranged LRPM qualitatively shows the same phase diagram, including tricriticality. In accordance with the results of Fig. 4, the tricritical point moves upwards to higher temperatures for larger odd values of r_{cut}/σ ; however, the topology of the phase diagram is not affected. It has already been mentioned that for even values of the cut-off radius r_{cut}/σ no charge-ordered phase is present so that a phase separation occurs between a charge-disordered gas and a charge-disordered liquid, and the phase diagram exhibits an ordinary critical point and no λ -line. Since the phase diagrams for even-valued cut-off radii are qualitatively different from that of the long-ranged LRPM they are not shown in Fig. 5.

B. Minimum image approximation (MIA)

When discussing the sharp cut-off schemes, i.e., with decay constant $\alpha = 0$ in Eq. (1), in the previous Subsec. III A, cut-off radii $r_{\text{cut}}/\sigma \leq (L - 1)/2$ have been assumed throughout. The phase diagram for odd values of the cut-off radius $r_{\text{cut}}/\sigma \leq (L - 1)/2$ turned out to be qualitatively identical to the phase diagram of the conventional long-ranged LRPM, but the tricritical point is located at a too high temperature T_c^* , which even increases upon increasing r_{cut} . Here, another sharp cut-off scheme is discussed which, in the notation of Eq. (1), can be specified by $\alpha = 0, q = \infty, r_{\text{cut}}/\sigma = (L - 1)/2$. This

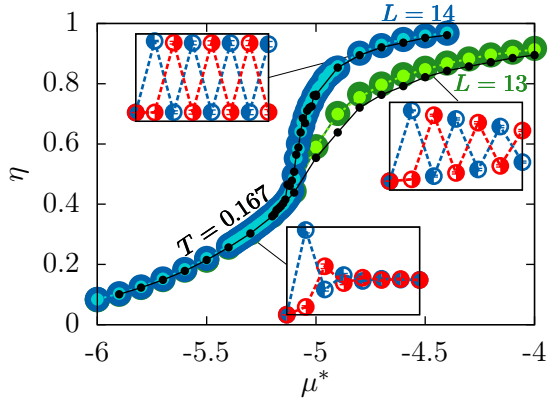


FIG. 6. Comparison of the equations of state and of the pair distribution functions for odd and even box sizes L . The green and blue dots in the main plot correspond to results within MIA ($p = 2, q = \infty, \alpha = 0, r_{\text{cut}}/\sigma = (L - 1)/2$ in Eq. (1)) and the black dots are obtained by means of the Ewald method. The same odd-even-effect of L in the high-density regime is encountered within both methods. Furthermore, the high-density phase displays decorrelations in the case of odd values of L , whereas the charge ordering is long-ranged in the case of even values of L . The occurrence of decorrelations in the high-density phase for odd-valued L can be understood in terms of equally charged ions at the rim of the simulation box, which interact with each other due to periodic boundary conditions.

cut-off scheme is equivalent to the well-known minimum image approximation (MIA) [37, 38], which disregards all contributions to the interaction energy, which do not correspond to the minimum distance between two ions or their periodic images. For a cubic simulation box, it can be interpreted such that only those interactions within a cut-off distance $\|\mathbf{r}\|_{\infty} \leq r_{\text{cut}}$ are taken into account, where the cut-off radius r_{cut} has to be chosen such that the interaction range equals a cube of volume L^3 with $L = 2r_{\text{cut}}/\sigma + 1$. Note, that the distances, which determine interaction potential, are measured in the p -norm (see Eq. (1)), which is chosen as $p \in \{1, 2\}$.

Figure 4 also displays the critical temperatures T_c^* within MIA for $p = 2$, which are in excellent agreement with the critical temperature $\Theta_c^* \in [0.14, 0.16]$ of the long-ranged LRPM. Moreover, the MIA results in Fig. 4 can be subdivided into integer and half-integer values of r_{cut}/σ , which corresponds respectively to odd and even values of the box size $L = 2r_{\text{cut}}/\sigma + 1$. A close look at Fig. 4 reveals that the values of T_c^* within MIA for odd values of L are slightly below those for even values of L , which indicates a certain odd-even effect of L on T_c^* . Whereas the odd-even effect of L on T_c^* is rather weak, Fig. 6 shows for the examples $L = 13$ and $L = 14$ that there is a significant odd-even effect of L on the equation of state and on the structure at large packing fractions. The reason for mentioning the odd-even effects of L within MIA here is that exactly the same odd-even effects of L occur for the long-ranged LRPM using the full Ewald method, which are shown in Fig. 6, too. In

other words, MIA is such a good approximation of the full Ewald method that it exhibits even the same odd-even effects.

The insets in Fig. 6, which show the pair distribution functions at the indicated thermodynamic states, reveal a distinct charge-ordering behavior in the high-density regime for even box sizes L , whereas for odd L a decaying oscillatory behavior of the pair distribution functions can be observed. Although the latter behavior does not correspond to a genuine charge-ordered phase, it is clearly different from the structure in the dilute regime, where correlations decay rapidly. What is the reason for this qualitatively different high-density structure for even and odd box sizes L ? In the limit of perfect charge-ordering at sufficiently high densities, the periodic boundary conditions lead to destabilizing contributions to the interaction energy for odd values of L , since in this case there are equally charged ions located at the rim of the simulation box which, due to the periodicity, are nearest neighbors. This effect does not occur for even box sizes L . Since this is obviously an effect related to the ‘surface’ of the simulation box, it decreases with increasing box size L . The same odd-even dependence of the equation of state and of the structure is observable within the long-ranged LRPM. As a consequence of the above argumentation, the results for even box sizes L , whether using MIA or the full Ewald method, can be expected to be more accurate, than for odd box sizes L .

It is striking that isotherms within MIA sample the long-range limit $r_{\text{cut}} \rightarrow \infty$ very well for dilute as well as for dense systems. This indicates that the Hamiltonian of an ionic fluid with long-ranged Coulomb interaction can be reliably approximated by Eq. (2) with $p = 2, q = \infty, \alpha = 0, r_{\text{cut}}/\sigma = (L - 1)/2$ in Eq. (1). In fact, for $L = 14$, there is almost no difference between MIA and the full Ewald method with respect to the equations of state (see Fig. 6).

This quantitative agreement can be understood as follows: The contribution to the energy due to the long-ranged Coulomb potential beyond MIA involves the electrostatic interaction of the simulation box with its images, which, due to the charge neutrality of the simulation box, decays at least as a dipole-dipole interaction, i.e., $\propto 1/r^3$. However, numerical calculations reveal that the dipole-dipole contribution vanishes and that the decay is actually $\propto 1/r^4$, which renders the long range contributions beyond MIA absolutely convergent and, for sufficiently large L , small. The same argument does not apply to the sharp cut-off potentials of Subsec. III A, since no charge neutrality inside spheres of radius r_{cut} within the underlying norm is guaranteed so that the long range contributions beyond those due to the sharp cut-off potential are due to an effective monopole-monopole interaction, i.e., $\propto 1/r$, and, hence, typically not small.

Figure 7 displays the phase diagram within MIA for $r_{\text{cut}}/\sigma = 4.5$; those for $r_{\text{cut}}/\sigma \in \{6, 6.5, 9\}$ obtained similarly are not shown here. For all considered cases of r_{cut} , the phase diagrams are qualitatively and quantita-

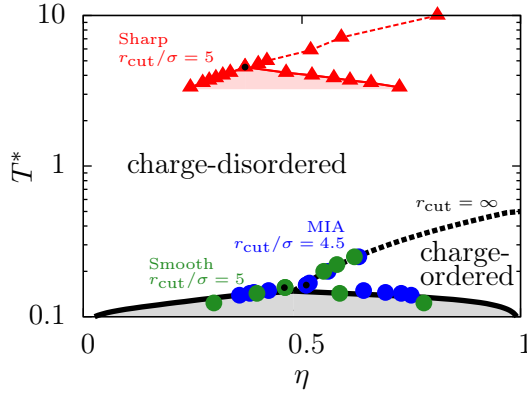


FIG. 7. Comparison of the phase diagrams of the LRPm within the sharp cut-off scheme $p = q = 1, \alpha\sigma = 0, r_{\text{cut}}/\sigma = 5 \leq (L-1)/2$ in Eq. (1), the MIA ($p = 2, q = \infty, \alpha\sigma = 0, r_{\text{cut}}/\sigma = 4.5 = (L-1)/2$), the smooth cut-off scheme ($p = q = 2, \alpha\sigma = 0.8, r_{\text{cut}}/\sigma = 5 \leq (L-1)/2$), and the long-ranged Coulombic interaction ($\alpha\sigma = 0, r_{\text{cut}} = \infty$). The agreement of the MIA and the smooth cut-off scheme with the case of the long-ranged interaction is excellent, whereas there are large quantitative deviations of the sharp cut-off scheme with $r_{\text{cut}}/\sigma \leq (L-1)/2$.

tively in accordance with those obtained by means of the corresponding full Ewald method. The important point is that the MIA can be interpreted as a sharp cut-off truncation scheme of the Coulomb potential. The results discussed above indicate that the long-range character of the electrostatic interaction may not be necessary for the thermal and structural properties of ionic fluids, because there is the possibility that the same properties can be generated by suitable short-ranged interactions. A comparison of the MIA, where $r_{\text{cut}}/\sigma = (L-1)/2$, with the sharp cut-off schemes of the previous Subsec. III A, where $r_{\text{cut}}/\sigma \leq (L-1)/2$, reveals that the ability of a sharp cut-off scheme to mimic the properties of the long-ranged LRPm depends delicately on the relation between the cut-off radius r_{cut} and the size of the simulation box L . However, the simulation box L is not a physical but rather a technical parameter, and the properties of the LRPm within reasonable sharp cut-off schemes Eq. (1) with $\alpha = 0$ should be independent of (large values of) L . Consequently, there are no sharp cut-off schemes which quantitatively reproduce the thermal and structural properties of the long-ranged LRPm and which, at the same time, correspond to physically acceptable underlying short-ranged interactions.

C. Smooth cut-off potentials

It turned out in the previous Subsec. III B that there are sharp cut-off schemes, i.e., with $\alpha = 0$ in Eq. (1), which, although based on a short-ranged potential Eq. (1), lead to quantitatively identical thermal

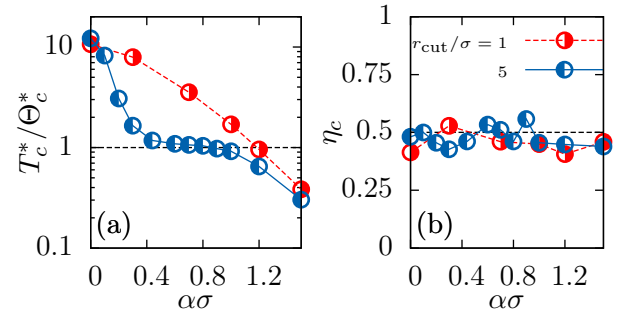


FIG. 8. Critical temperature T_c^* and critical packing fraction η_c of the LRPm with smooth cut-off potentials Eq. (1) with $p = q = 2, L = 12, r_{\text{cut}}/\sigma \in \{1, 5\}$ as functions of the decay constant $\alpha\sigma$. For $r_{\text{cut}}/\sigma = 5$ the critical temperature T_c^* exhibits a plateau around $\alpha\sigma \approx 0.8$ which is close to the critical temperature Θ_c^* of the long-ranged Coulombic system. As in Figs. 4, 5, and 7, the critical temperature T_c^* within sharp cut-off schemes ($\alpha\sigma = 0$) is an order of magnitude too high. The critical packing fraction $\eta_c \approx 0.5$ is rather independent of the decay constant α and the cut-off radius r_{cut} .

and structural properties as the conventional LRPm with the long-ranged Coulomb potential. However, these sharp cut-off schemes do not correspond to physical systems, because one has to tune the cut-off radius r_{cut} according to the unphysical simulation box size L , whereas for physically acceptable short-ranged potentials r_{cut} should be independent of L . Here, potentials Eq. (1) with $\alpha > 0$ are considered, which correspond to a smooth cutting off of the Coulomb potential on the length scale $1/\alpha$. Note, that this type of functions occurs within the Ewald method as a result of splitting the total electrostatic potential into a short-ranged contribution, which leads to a sum in real space, and a long-ranged contribution, which leads to a sum in reciprocal space. Within the Ewald method, α is adjusted such that, on the one hand, the error due to the unavoidable truncation of the sums in real and reciprocal space are sufficiently small and that, on the other hand, the computational effort is acceptable. However, here α controls the decay length of a genuine short-ranged interaction, which can take, in principle, any (positive) value. For $\alpha \rightarrow 0$ the sharp cut-off truncation schemes discussed in Sec. III A are obtained.

Figure 8 displays the critical temperature T_c^* and the critical packing fraction η_c of the LRPm with smooth cut-off potentials Eq. (1) with $p = q = 2, r_{\text{cut}}/\sigma \in \{1, 5\}$ as functions of the decay constant $\alpha\sigma$. For $r_{\text{cut}}/\sigma = 5$ a plateau of T_c^* is present in the range $\alpha\sigma \in [0.4, 1.0]$, where the critical temperature T_c^* is quantitatively equivalent to the critical temperature Θ_c^* of the long-ranged LRPm (see Fig. 8(a)). For larger values of $\alpha\sigma$ the decay length of the interaction Eq. (1) becomes too short, so that even nearest neighbors barely interact with each other. Hence, for $\alpha\sigma \rightarrow \infty$, one obtains the ideal gas limit and consequently $T_c^* \rightarrow 0$. For $r_{\text{cut}}/\sigma = 1$ all contributions beyond the nearest neighbors are neglected, and no plateau is

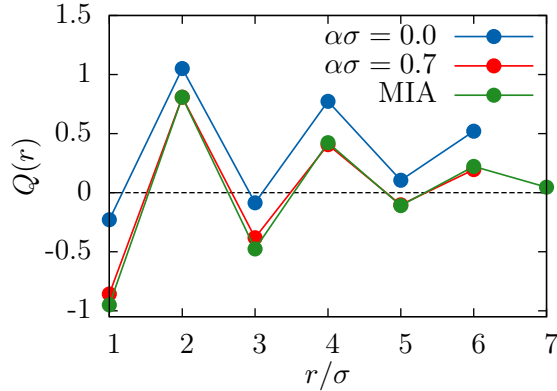


FIG. 9. Accumulated charge $Q(r)$ (see Eq. (7)) up to a distance r in 1-norm around a positively charged central ion. The Stillinger-Lovett sum rule [13–16] requires $Q(r)$ to vanish in the limit of large distances $r \rightarrow \infty$. This condition appears to be fulfilled within the charge-disordered phase (here at packing fraction $\eta \approx 0.3$) for the case of the smooth cut-off potential $\alpha\sigma = 0.7$ ($p = q = 2, r_{\text{cut}}/\sigma = 5, L = 12$) as well as for the MIA ($\alpha\sigma = 0, p = 2, q = \infty, r_{\text{cut}}/\sigma = 6.5 = (L-1)/2, L = 14$), but not for the sharp cut-off potential $\alpha\sigma = 0$ ($p = q = 2, r_{\text{cut}}/\sigma = 1, L = 12$).

observable at all. However, the critical packing fraction $\eta_c \approx 0.5$ appears to be independent of the decay constant α and the cut-off radius r_{cut} . In addition to the coincidence of the critical points for the appropriate choice of $\alpha\sigma$, a charge-ordered phase at large packing fractions and a charge-disordered phase at small packing fractions can be found. Ultimately, the phase diagrams of the smooth cut-off scheme are in quantitative agreement with the long-ranged limit, too (see Fig. 7).

The long-range character of the Coulomb interaction is well-known to generate the so-called Stillinger-Lovett perfect screening property of ionic fluids [13–18]. In the present context of an LRPM it corresponds to the accumulated charge

$$Q(r) := 1 + \frac{\eta}{2} \sum_{\substack{\mathbf{r}' \in \mathcal{V} \\ 1 \leq \|\mathbf{r}'\|_1 \leq r}} [g_{\oplus, \oplus}(\mathbf{r}') - g_{\oplus, \ominus}(\mathbf{r}')] \quad (7)$$

up to a 1-norm distance r around a positively charged central ion to vanish $Q(r) \rightarrow 0$ in the limit $r \rightarrow \infty$. Figure 9 compares the accumulated charge $Q(r)$ for the sharp cut-off potential with $\alpha\sigma = 0, r_{\text{cut}}/\sigma = 1, p = q = 2$, the MIA with $\alpha\sigma = 0, r_{\text{cut}}/\sigma = 6.5, p = 2, q = \infty$ and the smooth cut-off potential $\alpha\sigma = 0.7, r_{\text{cut}}/\sigma = 5, p = q = 2$ within the charge-disordered phase at packing fraction $\eta \approx 0.3$. For the sharp cut-off potential, $Q(r)$ appears to converge towards a non-vanishing (positive) value for large radii r , which corresponds to an imperfect screening of the positive central charge. However, perfect screening occurs within the MIA and the smooth cut-off potential. This is an interesting finding since, in contrast to the long-range Coulomb potential, the perfect screen-

ing property is not necessarily fulfilled in systems with short-ranged interactions.

It can be shown for smoothly cut-off potentials Eq. (1) with $r_{\text{cut}}\alpha \gg 1$ that the charge-charge pair correlation function $h_{zz}(r) := 2(g_{\oplus, \oplus}(r) - g_{\oplus, \ominus}(r))$, which is related to the accumulated charge $Q(r)$ in Eq. (7), decays asymptotically on the length scale of the Debye length $1/\kappa$ with $(\kappa\sigma)^2 = 4\pi\eta/T^*$ iff $\kappa \gg 2\alpha$. Since $\alpha > 0$ is a constant, which is chosen to match the phase diagram of the long-ranged Coulomb interaction (see Figs. 7 and 8) and which does not depend on the thermodynamic state (η, T^*) , the condition $\kappa \gg 2\alpha > 0$ will not be fulfilled at very low packing fractions η and/or high temperatures T^* , i.e., the Debye-Hückel limit is not recovered within smooth cut-off schemes. However, we do not consider this a major defect for two reasons: On the one hand, the remaining parts of the phase diagram outside the region of the Debye-Hückel limit, particularly in the range of high densities, e.g., close to the critical point ($\eta_c \approx 0.5$), are reproduced quantitatively (see Figs. 7 and 8). On the other hand, the crossover, where the condition $\kappa \gg 2\alpha$ begins to be violated, can be shifted to arbitrarily small values of κ by decreasing α , which can be achieved by accordingly increasing r_{cut} (see Fig. 8(a)).

Concerning the phase behavior and the structure, the LRPM with the smooth cut-off potentials considered here is qualitatively equivalent to that with long-ranged Coulomb interactions. Moreover, by choosing an appropriate decay constant α , the short-ranged smooth cut-off potential LRPM becomes even quantitatively equivalent to the conventional long-ranged LRPM. The essential difference to the sharp cut-off schemes considered in Subsecs. III A and III B is that these statements are independent of the choice of the actual (large) value of the simulation box L , i.e., the smooth cut-off potentials discussed here are candidates of physically meaningful short-ranged interactions. Consequently, the long-range character of the electrostatic potentials is of minor importance for the thermal and structural properties of ionic fluids, since, as has been demonstrated here, short-ranged interaction potentials do exist, which lead to the same thermal and structural properties.

IV. CONCLUSIONS AND SUMMARY

In order to elucidate the role of the long-range character of the Coulomb potential for the thermodynamic and the structural properties of ionic fluids, the lattice restricted primitive model (LRPM) with various truncated Coulomb-like interaction potentials Eq. (1) has been studied in this work by means of grandcanonical Monte Carlo simulations.

The simplest approach of sharply truncating the Coulomb potential at a certain cut-off radius r_{cut} (Sec. III A) turned out to be not appropriate to reproduce the properties of the long-ranged LRPM, either qualitatively or quantitatively. When measuring distances

within the 1-norm, e.g., no charge-ordered phase occurs for even-valued cut-off radii r_{cut}/σ , i.e., the topology of phase diagram differs from that of the conventional long-ranged LRPM. On the other hand, odd-valued cut-off radii lead to qualitatively the same phase diagrams as the conventional long-ranged LRPM (Fig. 5), but there is a large quantitative difference, e.g., of the value of the critical temperature T_c^* (Fig. 4).

In contrast, the well-known minimum image approximation (MIA), which may be viewed as a sharp cut-off scheme with the cut-off radius r_{cut} being related to the side length of the simulation box L , leads to quantitative agreement of the phase behavior and the structure of the LRPM with that of the long-ranged LRPM (Fig. 7).

However, due to the relation of the cut-off radius with the unphysical parameter L , the MIA does not correspond to a physically acceptable, i.e., L -independent,

short-ranged potential. Quantitative agreement of the phase behavior and the structure of short-ranged and long-ranged LRPMs is achieved by smoothly cutting off the Coulomb interaction, which is expressed by a decay constant α , corresponding to a decay length of $1/\alpha$ (Fig. 8). Interestingly, the LRPM with the smoothly cut off Coulomb potential possesses, although it is based on short-ranged potentials, the Stillinger-Lovett perfect screening property (Fig. 9).

By showing that the characteristic phase behavior and structure of ionic fluids can also be found in systems with short-ranged potentials, one can conclude that the decisive property of the electrostatic potential in ionic fluids is not the long range but rather the valency dependence. As this conclusion is drawn from a study of the LRPM, the natural question arises whether it holds for off-lattice models, too. This task is left for future investigations.

-
- [1] W. Liu, C. Ye, Q. Gong, H. Wang, and P. Wang, *Tribo. Lett.* **13**, 81 (2002).
 - [2] Y. U. Paulechka, G. J. Kabo, A. V. Blokhin, O. A. Vydrov, J. W. Magee, and M. Frenkel, *J. Chem. Eng. Data* **48**, 457 (2003).
 - [3] M. D. Bermúdez, A. E. Jiménez, J. Sanes, and F. J. Carrión, *Molecules* **14**, 2888 (2009).
 - [4] M. Bier and S. Dietrich, *Mol. Phys.* **108**, 211 (2010).
 - [5] N. Yamanaka, R. Kawano, W. Kubo, N. Masaki, T. Kitamura, Y. Wada, M. Watanabe, and S. Yanagida, *J. Phys. Chem. B* **111**, 4763 (2007).
 - [6] P. Wasserscheid and T. Welton, *Ionic Liquids in Synthesis*, Vol. 2 (Wiley-VCH, Weinheim, 2007).
 - [7] T. L. Greaves and C. J. Drummond, *Chem. Rev.* **108**, 206 (2008).
 - [8] M. Armand, F. Endres, D. R. MacFarlane, H. Ohno, and B. Scrosati, *Nature Mater.* **8**, 621 (2009).
 - [9] S. Tan and D. R. MacFarlane, in *Ionic Liquids*, Topics in Current Chemistry, Vol. 290 (Springer, Berlin, Heidelberg, 2010) Chap. 35, pp. 311–339.
 - [10] T. Yasuda and M. Watanabe, *MRS Bull.* **38**, 560 (2013).
 - [11] H. Wang, Q. Lu, C. Ye, W. Liu, and Z. Cui, *Wear* **256**, 44 (2004).
 - [12] A. Suzuki, Y. Shinka, and M. Masuko, *Tribo. Lett.* **27**, 307 (2007).
 - [13] F. H. Stillinger and R. Lovett, *J. Chem. Phys.* **48**, 3858 (1968).
 - [14] R. Lovett and F. H. Stillinger, *J. Chem. Phys.* **48**, 3869 (1968).
 - [15] F. H. Stillinger and R. Lovett, *J. Chem. Phys.* **49**, 1991 (1968).
 - [16] J. P. Hansen and I. R. McDonald, *Theory of Simple Liquids* (Academic Press, London, 1976).
 - [17] D. Mitchell, D. A. McQuarrie, A. Szabo, and J. Groeneveld, *J. Stat. Phys.* **17**, 15 (1977).
 - [18] P. Martin and C. Gruber, *J. Stat. Phys.* **31**, 691 (1983).
 - [19] M. E. Fisher, *J. Stat. Phys.* **75**, 1 (1994).
 - [20] B. P. Lee and M. E. Fisher, *Phys. Rev. Lett.* **76**, 2906 (1996).
 - [21] V. Kobelev, A. B. Kolomeisky, and M. E. Fisher, *J. Chem. Phys.* **116**, 7589 (2002).
 - [22] S. Wiegand, J. M. H. Levelt Sengers, K. J. Zhang, M. E. Briggs, and R. W. Gammon, *J. Chem. Phys.* **106**, 2777 (1997).
 - [23] S. Wiegand, M. E. Briggs, J. M. H. Levelt Sengers, M. Kleemeier, and W. Schröer, *J. Chem. Phys.* **109**, 9038 (1998).
 - [24] S. Wiegand, R. F. Berg, and J. M. H. Levelt Sengers, *J. Chem. Phys.* **109**, 4533 (1998).
 - [25] H. L. Bianchi and M. L. Japas, *J. Chem. Phys.* **115**, 10472 (2001).
 - [26] Q. Yan and J. J. de Pablo, *J. Chem. Phys.* **114**, 1727 (2001).
 - [27] E. Luijten, M. E. Fisher, and A. Z. Panagiotopoulos, *Phys. Rev. Lett.* **88**, 185701 (2002).
 - [28] A. Z. Panagiotopoulos, *J. Chem. Phys.* **116**, 3007 (2002).
 - [29] Y. C. Kim and M. E. Fisher, *Phys. Rev. Lett.* **92**, 185703 (2004).
 - [30] R. Dickman and G. Stell, *AIP Conf. Proc.* **492**, 225 (1999).
 - [31] R. Ren, C. J. O’Keeffe, and G. Orkoulas, *J. Chem. Phys.* **125**, 124504 (2006).
 - [32] P. P. Ewald, *Ann. Phys. (Leipzig)* **369**, 253 (1921).
 - [33] V. Privman, *Finit-Size Scaling Theory and Numerical Simulation of Statistical Systems* (World Scientific, Singapore, 1990).
 - [34] A. M. Ferrenberg and R. H. Swendsen, *Phys. Rev. Lett.* **61**, 2635 (1988).
 - [35] A. K. Jain and D. P. Landau, *Phys. Rev. B* **22**, 445 (1980).
 - [36] A. Z. Panagiotopoulos and S. K. Kumar, *Phys. Rev. Lett.* **83**, 2981 (1999).
 - [37] N. Metropolis, A. W. Rosenbluth, M. N. Rosenbluth, A. H. Teller, and E. Teller, *J. Chem. Phys.* **21**, 1087 (1953).
 - [38] D. N. Card and J. P. Valleau, *J. Chem. Phys.* **52**, 6232 (1970).